# Impacts of Heterogeneous Organic Matter on Phenanthrene Sorption: Equilibrium and Kinetic Studies with Aquifer Material

**ARTICLE** *in* ENVIRONMENTAL SCIENCE AND TECHNOLOGY · DECEMBER 1999

Impact Factor: 5.33 · DOI: 10.1021/es9902219



**5 AUTHORS**, INCLUDING:

Hrissi K Karapanagioti
University of Patras
**65** PUBLICATIONS **1,112** CITATIONS
SEE PROFILE

David Alan Sabatini
University of Oklahoma
**212** PUBLICATIONS **4,830** CITATIONS
SEE PROFILE

Peter Grathwohl
University of Tuebingen
**279** PUBLICATIONS **4,476** CITATIONS
SEE PROFILE

Bertrand Ligouis
University of Tuebingen
**37** PUBLICATIONS **865** CITATIONS
SEE PROFILE

*Environ. Sci. Technol.* **2000**, *34,* 406−414

# Impacts of Heterogeneous Organic Matter on Phenanthrene Sorption: Equilibrium and Kinetic Studies with Aquifer Material

HRISSI K. KARAPANAGIOTI,[†]
SYBILLE KLEINEIDAM,[‡]
DAVID A. SABATINI,*[,†]
PETER GRATHWOHL,[‡] AND
BERTRAND LIGOUIS[‡]

*School of Civil Engineering and Environmental Science, University of Oklahoma, Norman, Oklahoma 73019, and Geological Institute, Applied Geology Group, University of Tübingen, Tübingen, Germany*

Sediment organic matter heterogeneity in sediments is shown to impact the sorption behavior of contaminants. We investigated the sorptive properties as well as the composition of organic matter in different subsamples (mainly grain size fractions) of the Canadian River Alluvium (CRA). Organic petrography was used as a new tool to describe and characterize the organic matter in the subsamples. The samples studied contained many different types of organic matter including bituminous coal particles. Differences in sorption behavior were explained based on these various types of organic matter. Subsamples containing predominately coaly, particulate organic matter showed the highest $K_{oc}$, the highest nonlinearity of sorption isotherms and the slowest sorption kinetics. Soil subsamples with organic matter present as organic coatings around the quartz grains evidenced the lowest $K_{oc}$, the most linear sorption isotherms and the fastest sorption kinetics, which was not limited by slow intraparticle diffusion. Due to the high sorption capacity of the coaly particles even when it is present as only a small fraction of the composite organic content (<3%) causes $K_{oc}$ values which are much higher than expected for soil organic matter (e.g. $K_{oc} - K_{ow}$ relationships). The results show that the identification and quantification of the coaly particles within a sediment or soil sample is a prerequisite in order to understand or predict sorption behavior of organic pollutants.

## Introduction

Natural attenuation is currently one of the most important topics in groundwater remediation. Sorption equilibrium and sorption/desorption kinetic properties are very important factors affecting natural attenuation of contaminants in the subsurface. While an extensive body of literature discusses sorption processes, little information considers the impact of heterogeneous organic matter on sorption properties.

Karickhoff et al. (*1*) published one of the earlier and more important studies on sorption of hydrophobic organic compounds. Instantaneous equilibrium and linear sorption isotherms were observed and attributed to partition-like sorption. The organic-content-normalized distribution coefficient ($K_{oc}$) was dependent on chemical hydrophobicity and solubility, as quantified by the chemical's octanol−water partition coefficient ($K_{ow}$). These observations have been corroborated for numerous media and organic contaminants (*2, 3,* and as summarized in ref *4*). Organic matter was assumed to be homogeneous and uniformly distributed, with the fraction organic carbon content ($f_{oc}$) viewed as adequate for characterization processes. However, select studies have shown that a minor fraction of a sample can govern sorption behavior of the bulk sample (*5, 6*). Other studies have demonstrated that the nature of the organic matter also has a significant impact on sorption capacity and nonlinearity (*7*−*12*). A correlation between $K_{oc}$ and O/H ratios illustrated the importance of soil organic matter quality on sorption capacity (*8, 13*).

A conceptual model of organic matter domains (soft or rubbery or amorphous and hard or glassy or condensed) has been presented, with each type of sorbent assigned qualitative sorption characteristics (*9, 10, 14,* summarized in ref *4*). A transition between the two organic matter domains was found (*15*), although their sorption characteristics are still not well established (*16*). Recently, the presence of other organic matter phases (e.g. high-surface-area carbonaceous material, soot, etc.) has been proposed as cause of nonlinear sorption and increased $K_{oc}$ values (*11, 17, 18*). Kleineidam et al. (*19*) characterized organic matter heterogeneity in sedimentary rocks and related organic matter facies to equilibrium sorption properties. Recently, Xia and Ball (*12*) proposed a model that accounts for adsorption and partitioning sorption sites to treat different sorption characteristics. In this specific model adsorption/pore filling is important at low contaminant concentrations while partitioning dominates sorption behavior at higher concentrations. The Polanyi-Manes approach was successful to model such a concept.

Sorption nonequilibrium can be attributed to intraparticle diffusion (*20*−*22*). Recent review papers summarize the slow sorption/desorption of organic compounds in natural particles (*4, 23*). Intraparticle pore diffusion models have been used to describe the long-term sorption kinetics in bulk samples (*20, 24, 25*). Rügner et al. (*22*) used an empirical correlation that predicts long-term sorption kinetics of organic pollutants based on intraparticle porosity and equilibrium sorption capacity of homogeneous constituents of a heterogeneous aquifer material.

The objectives of this study were as follows: (1) to examine the effects of heterogeneous organic matter on sorption equilibria and kinetic parameters in a sandy aquifer material, (2) to relate variations in sorption properties with characteristics of the organic matter type, and (3) to model the kinetic results using an intraparticle diffusion model (numerical solution of Fick's 2nd law). Variations in equilibrium sorption parameters and sorption kinetics for soil subsamples were explained based on the organic matter characteristic present. This study is unique in demonstrating the presence of heterogeneous organic matter in alluvial aquifer materials (e.g. coal, charcoal, amorphous organic matter, etc.), characterizing these different components and quantifying their impact on sorption properties.

## Materials and Methods

The Canadian River Alluvial (CRA) aquifer material was sampled from the closed Norman Landfill, which is a U.S.G.S. Toxic Substances Research site. The sampling depth was just

* Corresponding author phone: (405)325-4273; fax: (405)325-4217; e-mail: sabatini@mailhost.ecn.ou.edu.
[†] University of Oklahoma.
[‡] University of Tübingen.


10.1021/es9902219 CCC: $19.00 
Published on Web 12/18/1999

**TABLE 1. Soil Subsamples and Organic Matter Characteristics[a]**

| | | | particulate organic matter (POM) | | | clay matrix (M) | | organic coating (C) |
|---|---|---|---|---|---|---|---|---|
| sample code | grain size (mm) | magnetic separation | coal (CL) | charcoal (CH) | phytoclast (PH) | POM | amorphous organic matter (AOM) | AOM |
| code | | | $POM_{CL}$ | $POM_{CH}$ | $POM_{PH}$ | $M_{POM}$ | $M_{AOM}$ | $C_{AOM}$ |
| CRA comp | ≤0.5 | none | | x | x | | x | x |
| $0.5M_{AOM}POM_{PH}$ | 0.5−0.25 | magnetic | x | | x | | x | |
| $0.5POM_{CL}$ | 0.5−0.25 | nonmagnetic | x | | x | | x | |
| $0.25POM_{PH}M_{POM}$ | 0.25−0.125 | magnetic | | | x | 1 $\mu$m[b] | | |
| $0.25M_{POM}$ | 0.25−0.125 | nonmagnetic | | | | 1−3 $\mu$m[b] | | |
| $0.125C_{AOM}POM_{PH}$ | 0.125−0.063 | magnetic | | | x | 5 $\mu$m[b] | x | x |
| $0.125C_{AOM}$ | 0.125−0.063 | nonmagnetic | | | | | | x |
| $0.063POM_{CH}C_{AOM}$ | ≤0.063 | magnetic | | x | | | | x |
| $0.063C_{AOM}POM_{CL}$ | ≤0.063 | nonmagnetic | x | | | | | x |
| presented in Figure 1, part: | | | a,c | b,c | d | c,e,f | c,e,f | g,h |

[a] Sample code: $XA_AB_B$ where: X: size fraction; $A_A$: most dominant organic matter characteristic; $B_B$: second dominant organic matter characteristic; POM: particulate organic matter with same particle size as the subsample grain size; M: clay matrix; C: organic coating; CL: coal; CH: charcoal; PH: phytoclast; AOM: amorphous organic matter; CRA comp: Canadian River Alluvium composite sample. [b] Instead of x that indicates presence numbers indicate POM diameter in the clay matrix.

below the water table at about 3 ft. The initial sample was divided into two groups with grain diameter size: (a) ≤0.5 mm and (b) >0.5 mm.

The smaller grain size sample was sieved into four subsamples (0.5−0.25 mm, 0.25−0.125 mm, 0.125−0.063 mm, ≤0.063 mm; nominally decreasing the radius by half for each size fraction) in order to assess the impact of grain radius on sorption kinetics. Each of these four grain size samples was then separated into two subsamples using a FRANTZ Magnetic Barrier Laboratory Separator Model LB-1 operated at 1.0 A, 10° longitudinal slope, and 0° lateral slope, resulting in a total of eight subsamples. Generally, the magnetic subsamples were dominated by quartz aggregates containing iron minerals in the clay matrices in the magnetic side, while individual quartz grains dominated the nonmagnetic samples. Magnetic separation of organic matter itself was not expected, unless the organic matter existed as isolated particles, single coal particles or wood residue. This procedure separated soil grains and organic matter associated in various forms to these grains (adsorbed, matrices etc.) due to magnetic properties of the grains and not due to organic matter properties. Coal is normally diamagnetic (*26*). Coal particles associated with pyrite were found in the two larger size fractions in the magnetic side. The presence of pyrite explains the paramagnetic properties of these coal particles. In the absence of pyrite it was not clear how and why magnetic separation would differentiate forms of organic matter. To characterize organic matter, polished thin sections of the soil subsamples were prepared. Microscopic investigations were carried out on a Leica DMRX photometer microscope. Organic matter was identified and characterized using white light and UV illumination in transmitted and reflected light mode. The soil organic matter characterization is done using a palynological classification (*27*). The observations were qualitative in nature; type and frequency (area covered in the thin section) of the organic matter present are summarized in Table 1.

Code names given to subsamples in Table 1 were based on their grain size and the dominant organic matter found in the thin sections. The subsamples were pretreated with HCl in order to remove inorganic carbon. The organic carbon content was then analyzed by dry combustion at 850 °C (Model 183 Boat Sampling Module, Rosemount) and quantified by an infrared detector for $CO_2$ (Horiba PIR-2000). Surface area and intraparticle meso-porosity were measured using $N_2$ and the BET method (ASAP 2010, Micromeritics) (more details on method are presented in ref *22*). The external surface area calculated based on the grain size was less than 0.1% of the specific surface area measured for all fractions.

Phenanthrene was used as the model chemical in this study. Phenanthrene ($C_{14}H_{10}$) is a three ring polycyclic aromatic hydrocarbon with (a) molecular weight: 178 g/mol, (b) solubility: 1.29 mg/L at 25 °C, (c) Henry's law constant: $2.6 \times 10^{-5}$ atm $m^3$/mol, and (d) log $K_{ow}$: 4.6 (*28*). The estimated log $K_{oc}$ of phenanthrene is 4.4 (*1*). Phenanthrene was chosen because of its high hydrophobicity ($K_{ow}$), low volatility (Henry's law constant), and simplicity of analysis. Phenanthrene was diluted to a 100 mg/L stock solution in methanol. Solutions were prepared in synthetic groundwater (deionized water with 44 mg/L $CaCl_2 \cdot 2H_2O$, 14 mg/L $CaSO_4$, and 17 mg/L $NaHCO_3$). Sodium azide ($NaN_3$) was added at a concentration of 200 mg/L to minimize bacterial growth and thus biodegradation during batch studies.

All equilibrium sorption experiments were conducted in triplicate in 10 mL crimp-top glass vials. Soil samples for equilibrium studies were pulverized to ensure equilibrium in a reasonable time (7 days). Variable phenanthrene concentrations were added to the soil samples and shaken for 7 days in the dark at constant temperature (20 °C). Headspace in the vials was kept to a minimum. Varying solid-to-water ratios were used based on different sorption capacities of the subsamples (i.e. to achieve sufficient sorption so that it could be easily quantified while keeping aqueous concentration above the detection limit). Samples were centrifuged at constant temperature of 20 °C before analysis.

All sorption kinetic experiments were conducted in triplicate in 100 mL crimp-top glass vials. The initial phenanthrene concentration was 0.1 mg/L, and the solid-to-water ratio was different for each subsample depending on the sorption capacity. The vials were stored at 20 °C in the dark and mixed periodically. Before analysis the samples were centrifuged at constant temperature of 20 °C. Measurements were taken at various time intervals. For both isotherm and kinetic batch experiments, aqueous phenanthrene concentrations were measured by a cuvette mode Perkin-Elmer LS-3B fluorescence spectrometer. To assess for fluorescent interferences some samples were analyzed in both UV and fluorescence detectors connected parallel to a HPLC system as well as the cuvette mode fluorescence detector. The results were comparable for all three detectors.

For each batch experiment blank samples were prepared and monitored (i.e., phenanthrene without soil). These blank samples did not indicate any significant phenanthrene degradation or sorptive losses on the glassware for the first 37 days. Some of the 30-day measurements showed large concentration differences between the triplicates, and these

data were not used for discussing the results. Although $NaN_3$ was present in all the reactors it did not prevent degradation completely, the $NaN_3$ did result in a lag period of about 15−30 days. To corroborate the onset of biodegradation all samples were solvent extracted with hot methanol at 60 °C for 4 days (*29*). For the triplicates that follow the diffusion model line the mass balance was within 90−100% recovery. Samples with a significantly lower recovery (26−76%) evidenced large deviations from the intraparticle diffusion model due to degradation losses (*30*).

## Data Modeling

The sorption distribution coefficient $K_d$ can be described by

$$K_d = q_e/C_e \quad (1)$$

where $q_e$ is the mass of chemical sorbed per unit mass of soil and $C_e$ is the equilibrium concentration. Nonlinear isotherms can be described by the Freundlich equation

$$q_e = K_{fr}C_e^{\,N} \quad (2)$$

where $K_{fr}$ is the Freundlich sorption constant and $N$ is the Freundlich exponent. For nonlinear isotherms $K_d$ can be considered concentration-dependent as follows:

$$K_d = K_{fr}C_e^{\,N-1} \quad (3)$$

The organic carbon content normalized distribution coefficient is described by

$$K_{oc} = K_d/f_{oc} \quad (4)$$

where $f_{oc}$ is the fraction organic carbon content of the sample. For nonlinear isotherms $K_{oc}$ is also concentration dependent. At a chemical concentration of unity, $K_d$ equals $K_{fr}$ and $K_{oc} = K_{fr}/f_{oc}$.

Solute diffusion from an aqueous phase into spherical porous grains can be described by Fick's 2nd law

$$\partial C/\partial t = D_a[(\partial^2 C/\partial r^2) + (2\partial C/r\partial r)] \quad (5)$$

where $C$ is the concentration of the chemical, $t$ is time, $D_a$ is the apparent diffusion coefficient, and $r$ is the radial distance from the center of the grain. In the intraparticle diffusion model $D_a$ is defined as

$$D_a = D_{aq}\epsilon/(\epsilon + K_d\rho)\tau_f \quad (6)$$

Where $D_{aq}$ is the aqueous diffusion coefficient, $\epsilon$ is the intraparticle porosity, $\rho$ is the bulk density of the grain, and $\tau_f$ is the tortuosity factor (*21*). In the present study, a numerical solution of Fick's 2nd law was utilized. The numerical model is based on the finite difference method using the Crank-Nicholson approach, as described by Jäger (*31*). Model input includes the grain radius, the solid-to-water ratio, the initial water concentration, the Freundlich parameters, the solid density, and the intraparticle porosity. In this study the numerical model was used to fit the sorption kinetic curves and produce values for $D_a/a^2$. Model calculations are based on minimizing the mean weighted squared errors between predicted and measured $K_d$ values. The sorptive uptake curves, expressed as normalized $K_d$ versus time, are relatively insensitive to different values of fractional uptake at equilibrium ($F$)—the chemical mass on solid per total chemical mass—and allow comparison of sorptive uptake at different solid-to-water ratios in batch experiments (*20*, summarized in ref *21*).

## Results and Discussion

**Soil Analysis.** Table 1 presents the code name and properties of each subsample (i.e., grain size, magnetic separation, and soil organic matter characterization). Other researchers have observed that $K_{oc}$ values differed for the magnetic separated fractions but have not characterized the organic matter in order to explain these findings (*32*, *33*). There are five basic types of organic matter present in our media: (a) coaly particulate organic matter (POM) (i.e. coal, charcoal) (Figure 1a−c), (b) young POM showing fluorescence in UV/blue light (i.e. phytoclast) (Figure 1a,d), (c) quartz aggregates with clay matrices containing coaly POM (Figure 1a,e,f), (d) quartz aggregates with clay matrices containing amorphous (in the palynological classification amorphous describes organic matter that lacks structure under the microscope) organic matter (AOM) in clay matrices (Figure 1a, e,f), and (e) grains with AOM coatings (Figure 1g,h). Each sample has one or two dominant organic matter characteristics. Coaly POM is contrasted to young POM by absence of fluorescence in blue reflected light under microscopy. Generally, fluorescence decreases with maturity and only AOM and young POM fluoresce (see Figure 1) (*27*).

Coal particles, present in all the samples, are believed to originate from coal seams in New Mexico, where the South Canadian River originates (Energy Resources Map of New Mexico, Map I-1327; U.S.G.S. and New Mexico Bureau of Mines and Mineral Resources, 1981). In one of the subsamples ($0.5M_{AOM}POM_{PH}$) the POM particles were counted visually and found to comprise 15% of the total grains in the subsample. However this percentage does not reflect weight percentages (wt %) because the organic particles are generally less dense than the soil particles. The $f_{oc}$, surface area, and porosity for each subsample and the bulk soil sample are presented in Table 2. Fine sand particles ($0.125C_{AOM}$) with AOM grain coatings make up 40 wt % of the composite sample but only contribute 9% of the organic carbon content for the composite sample. A large fraction (31%) of the composite sample $f_{oc}$ comes from a fraction that accounts for only 2.3 wt % of the composite sample ($0.5M_{AOM}POM_{PH}$). Subsamples with coaly POM are characterized by high organic content, while those dominated by AOM coatings of quartz grains are characterized by low organic content (Table 2). Samples dominated by coal particles have a small internal meso-pore range porosity ($0.5POM_{CL}$, $0.063M_{AOM}POM_{CL}$). Coal particles (CL) have a more uniform solid surface whereas phytoclast and charcoal are structured and highly porous particles (Figure 1). The presence of clay matrices explains the high porosity for samples where the organic matter is dominated by AOM in clay matrices.

**Equilibrium Sorption Isotherms.** Phenanthrene sorption isotherms demonstrated a Freundlich curvilinear shape, suggesting more than just partitioning of the chemical into the organic matter (some examples are given in Figure 2; note log−log plot with slope less than one indicating nonlinearity); this is true both for the composite sample and the subsamples. Freundlich parameters are presented in Table 3 for all samples. Sample ($0.125C_{AOM}$) shows some deviations from the Freundlich type isotherm in the upper concentration range, which is attributed to experimental error due to dilutions above the instrument linear range. The $K_{fr}$ value for the composite soil sample is not statistically different from the $K_{fr}$ value calculated based on integrating results for subsamples at the 95% confidence level {$(1100 \pm 170)$ versus $(1500 \pm 260)$, respectively}. A correlation of sorption behavior to organic matter characteristics can only be carried out based on the organic carbon normalized distribution coefficients ($K_{oc}$ values). Between all samples, $K_{oc}$ values (based on $K_d$ at $C_e$=1 $\mu$g/L) varied by 2 orders of magnitude ($\log K_{oc}$ of 4.7−6.3) and were always higher than $K_{ow}$-based estimates {$\log K_{oc} = 4.4$ (*1*)}. By estimating sorption parameters based on $K_{ow}$ it is automatically assumed that the organic matter is comparable with octanol and exhibits linear sorption isotherms, which is not true for any of the samples. Several

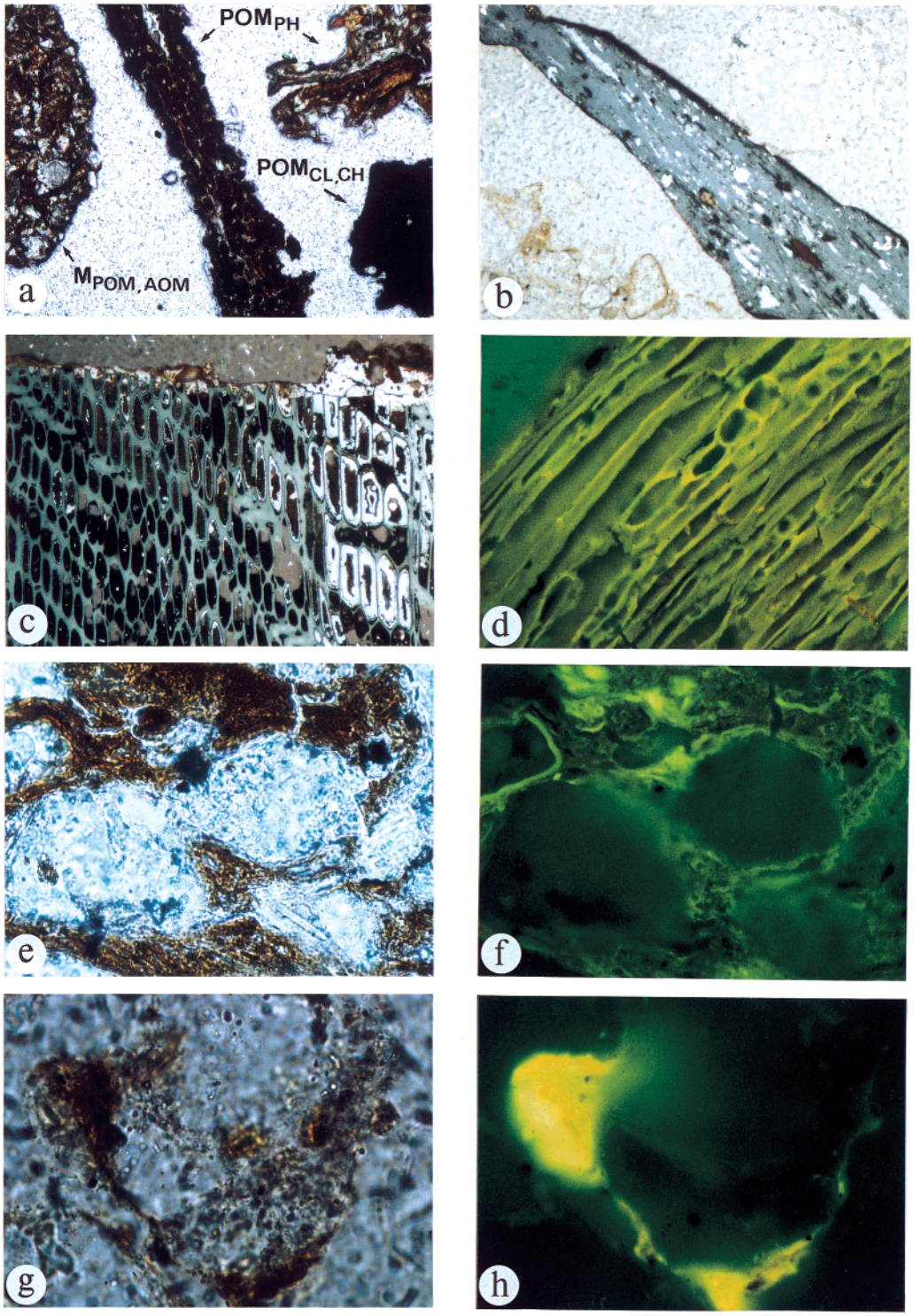


**FIGURE 1. Photomicrographs illustrating the different organic matter present in the samples: (a) overview of different particulate organic matter (POM). Brown phytoclasts ($POM_{PH}$), opaque particle—coal ($POM_{CL}$) or charcoal ($POM_{CH}$), and quartz aggregate with clay matrix containing amorphous organic matter ($M_{AOM}$) and POM ($M_{POM}$); transmitted white light (field 1.58 mm wide); (b) coal particle ($POM_{CL}$); polished surface, reflected white light, oil immersion, (field 406 $\mu$m wide); (c) charcoal particle ($POM_{CH}$), note the well preserved cellular structure, some of the wood cells are filled with sulfide; polished surface, reflected white light, oil immersion (field 406 $\mu$m wide); (d) phytoclast particle ($POM_{PH}$), the cell wall showing strong yellow-green fluorescence; incident light, fluorescence mode, oil immersion (field 158 $\mu$m wide); (e, f) e: quartz aggregates cemented with clay matrix (brown color); transmitted white light, oil immersion (field 158 $\mu$m wide), f: strong yellowish fluorescing AOM within the clay matrix ($M_{AOM}$), nonfluorescing small particles (black) are POM either coal or charcoal particles ($M_{POM}$); incident light fluorescence mode, oil immersion (field 158 $\mu$m wide); (g, h) g: isolated quartz mineral; transmitted white light, oil immersion (field 124 $\mu$m wide), h: strong yellow fluorescing organic coating ($C_{AOM}$); incident light fluorescence mode, oil immersion (field 124 $\mu$m wide). All pictures were taken with a Leitz DMRX microscope, equipped with a WILD MPS48 photoautomat. Filters for the incident light fluorescence mode (UV+V excitation): excitation 355—425 nm, beam splitter 455 nm and barrier 470 nm.**

researchers have presented results that disagree with $K_{ow}$ based predictions (*8, 11, 19, 33, 34*). The differences observed within the samples can be attributed to the nature of the organic matter present as discussed further below. The fact that $K_{oc}$ values are as much as 2 orders of magnitude greater than $K_{ow}$-based estimates demonstrate that partitioning into

**TABLE 2. Soil Analysis[a]**

| sample code | diameter (mm) | dominant organic matter | wt (%) | $f_{oc}$ (%) | fraction of composite $f_{oc}$ in subsample (%) | SA ($m^2$/g) | PV ($cm^3$/g) | intraparticle porosity ($\epsilon$) |
|---|---|---|---|---|---|---|---|---|
| CRA comp | ≤0.5 | mixture | 100 | 0.44 | 100 | 5.3 | 0.0067 | 0.017 |
| $0.5M_{AOM}POM_{PH}$ | 0.5−0.25 | AOM in clay matrix | 2.3 | 5.90 | 31 | 17.0 | 0.0220 | 0.055 |
| $0.5POM_{CL}$ | 0.5−0.25 | POM− coal | 0.75 | 1.60 | 3 | 1.7 | 0.0032 | 0.008 |
| $0.25POM_{PH}M_{POM}$ | 0.25−0.125 | POM− phytoclast | 5.3 | 1.30 | 16 | 12.0 | 0.0170 | 0.043 |
| $0.25M_{POM}$ | 0.25−0.125 | POM in clay matrix | 23 | 0.16 | 8 | 2.2 | 0.0031 | 0.008 |
| $0.125C_{AOM}POM_{PH}$ | 0.125−0.063 | AOM coating | 18 | 0.51 | 21 | 2.5 | 0.0089 | 0.023 |
| $0.125C_{AOM}$ | 0.125−0.063 | AOM coating | 40 | 0.10 | 9 | 3.1 | 0.0041 | 0.011 |
| $0.063POM_{CH}C_{AOM}$ | ≤0.063 | POM − charcoal | 6.6 | 0.76 | 11 | 12.0 | 0.0160 | 0.041 |
| $0.063C_{AOM}POM_{CL}$ | ≤0.063 | AOM coating | 4.4 | 0.18 | 2 | 3.3 | 0.0010 | 0.003 |

[a] Sample code: $XA_AB_B$ where X: size fraction; $A_A$: most dominant organic matter characteristic; $B_B$: second dominant organic matter characteristic; POM: particulate organic matter; CL: coal; CH: charcoal; PH: phytoclast; AOM: amorphous organic matter; M: clay matrix; C: coating; CRA comp: Canadian River Alluvium composite sample; wt %: weight fraction of subsample relative to composite; $f_{oc}$: organic carbon content; SA: surface area; PV: pore volume for pore diameter <66.6 nm; intraparticle porosity ($\epsilon$) = PV/(PV+1/$\rho$) (*32*) assuming that the bulk density of the grain ($\rho$) equals 2.65 g/$cm^3$.

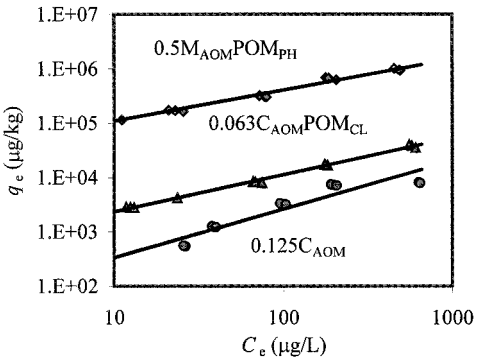


**FIGURE 2. Phenanthrene sorption isotherms for three subsamples. The chemical in the sorbed phase [$q_e$ ($\mu$g of chemical /kg of soil)] versus the chemical equilibrium concentration [$C_e$ ($\mu$g/L)] in solution. Sample code: $XA_AB_B$ where X: size fraction; $A_A$: most dominant organic matter characteristic; $B_B$: second dominant organic matter characteristic; M: clay matrix; AOM: amorphous organic matter; POM: particulate organic matter; PH: phytoclast; C: coating; CL: coal.**

organic carbon content alone is not enough to predict $K_{fr}$ values. Log $K_{oc}$ values were also calculated for a phenanthrene concentration of 1 mg/L; as concentrations approach solubility limits the $K_{oc}$ values approach $K_{ow}$-based estimates.

Figure 3 presents a plot of log $K_{oc}$ values versus Freundlich exponents ($N$) for low and high equilibrium phenanthrene concentration (1 $\mu$g/L and 1 mg/L, respectively). The plot demonstrates an apparent inverse relation between log $K_{oc}$ and $N$ for low equilibrium concentrations (i.e. as $N$ increases, log $K_{oc}$ values decrease). For higher chemical concentrations (close to phenanthrene's solubility limit of 1.29 mg/L), log $K_{oc}$ values are almost the same for all subsamples and very close to the $K_{ow}$-based estimates (4.4). This observation is in agreement with Xia and Ball (*12*), who state that while at high concentrations linear partitioning dominates the sorption process and $K_{ow}$-based estimates are valid, at low concentrations a pore-filling process takes place resulting in overall nonlinear sorption isotherms. $K_{oc}$ and $N$ values depend on the processes involved and thus on the type of organic matter present, as further discussed below (see Table 3).

The lowest $N$ and highest $K_{oc}$ (log $K_{oc}$ = 6.3) values were found for the subsample dominated by coaly POM particles ($0.5POM_{CL}$), while the highest $N$ and lowest $K_{oc}$ (log $K_{oc}$ = 4.6) values were found for the subsample dominated by AOM coatings of quartz grains (see $0.125C_{AOM}$ in Table 3). It is obvious from the observed $K_{oc}$ values that coaly POM particles, even when present as only 3% of the composite organic matter, can contribute significantly to the overall sorption. The remaining subsamples show log $K_{oc}$ and $N$ values between these extremes (see Figure 3 and Table 3). For subsamples with organic matter consisting of both POM and AOM coatings, the highest $K_{oc}$ value corresponds to samples with the highest charcoal present ($0.063POM_{CH}C_{AOM}$), followed by the sample with coal ($0.063C_{AOM}POM_{CL}$), with phytoclasts present in the third sample ($0.125C_{AOM}POM_{PH}$). In the sample with coal particles present in clay matrices ($0.25M_{POM}$), the log $K_{oc}$ value is lower compared to the log $K_{oc}$ value for a sample with isolated coal particles ($0.5POM_{CL}$). While the sample ($0.5M_{AOM}POM_{PH}$) is dominated by AOM and phytoclasts, it contains some coaly particles as well (Table 1). Its high log $K_{oc}$ (5.7) reflects the presence of coaly POM; while coaly POM does not dominate the sample $f_{oc}$, it does dominate the sample reactivity. Mixed samples tend to have $K_{oc}$ and $N$ values more similar to the coaly particles even though they are present in low percentages. For a prediction of $K_{oc}$ values the quantification of the strongly sorbing coaly POM is essential. Our ongoing work is focusing on this topic. Gustafsson et al. (*18*) found up to 2 orders of magnitude difference between phenanthrene $K_{oc}$ with or without a $K_{oc}$ percentage for what they called a soot phase.

The low $N$ values associated with coal particles suggest that adsorption is dominant due to site limited-surface accumulation (*9*) and /or pore filling mechanism (*12*). Amorphous organic matter coatings of quartz grains produce the lowest $K_{oc}$ value and the most linear isotherm in this study, likely due to the partitioning-type process occurring into these coatings. While the presence of phytoclast particles (i.e. $0.5M_{AOM}POM_{PH}$, $0.25POM_{PH}M_{POM}$) also increases the organic content, phytoclast $K_{oc}$ values are not as high as that observed for coal particles. Phytoclast particles present more linear isotherms than coal, suggesting a partition-like mechanism. It has to be pointed out that even the lowest $K_{oc}$ value of this study (log $K_{oc}$ = 4.6−4.7; 95% confidence interval) is still significantly higher than $K_{ow}$-based estimates, likely due to the coaly POM present in all subsamples. The exact contribution of each organic matter component cannot be easily distinguished in these heterogeneous samples, and only overall trends are discussed.

**Sorption Kinetics.** Figure 4 presents the apparent sorption coefficient as a function of time ($K_{da}$) normalized by the equilibrium distribution coefficient ($K_d$) for three of the subsamples and also shows the numerical model results for these data. $K_d$ is the value extrapolated from the Freundlich equation based on the expected aqueous equilibrium concentration $\{K_{fr}C_e^{(N-1)} = [(C_o - C_e)V]/(C_eM)$ where $C_o$ is the initial concentration in solution, $V$ is the solution volume, and $M$ the mass of sediment$\}$. Table 4 presents results of experimental data and modeling work studying the kinetic sorption properties of the soil samples. The radii used in the model to fit the diffusion rate constant ($D_a/a^2$) were calculated

**TABLE 3. Isotherm Results[a]**

| sample code | wt (%) | $f_{oc}$ (%) | $N$ | $K_{fr}$ ($\mu$g/kg)(L/$\mu$g)$^N$ | obs | $R^2$ | log $K_{oc}$ at $C_e$ = 1 $\mu$g/L 95% CI | log $K_{oc}$ at $C_e$ = 1 mg/L 95% CI |
|---|---|---|---|---|---|---|---|---|
| CRA comp | 100 | 0.44 ± 0.027 | 0.65 ± 0.021 | 1100 ± 85 | 13 | 0.99 | 5.3−5.5 | 4.3−4.4 |
| $0.5M_{AOM}POM_{PH}$ | 2.3 | 5.90 ± 0.640 | 0.57 ± 0.020 | 30000 ± 2500 | 15 | 0.98 | 5.6−5.8 | 4.4−4.5 |
| $0.5POM_{CL}$ | 0.75 | 1.60 ± 0.076 | 0.55 ± 0.024 | 33000 ± 2100 | 15 | 0.98 | 6.3−6.4 | 4.9−5.1 |
| $0.25POM_{PH}M_{POM}$ | 5.3 | 1.30 ± 0.061 | 0.69 ± 0.033 | 2700 ± 350 | 15 | 0.97 | 5.3−5.4 | 4.3−4.5 |
| $0.25M_{POM}$ | 23 | 0.16 ± 0.014 | 0.74 ± 0.036 | 230 ± 37 | 15 | 0.97 | 5.1−5.2 | 4.3−4.5 |
| $0.125C_{AOM}POM_{PH}$ | 18 | 0.51 ± 0.007 | 0.73 ± 0.032 | 700 ± 92 | 15 | 0.98 | 5.1−5.1 | 4.2−4.4 |
| $0.125C_{AOM}$ | 40 | 0.10 ± 0.004 | 0.89 ± 0.091 | 43 ± 15 | 14 | 0.89 | 4.6−4.7 | 4.1−4.5 |
| $0.063POM_{CH}C_{AOM}$ | 6.6 | 0.76 ± 0.038 | 0.57 ± 0.019 | 2900 ± 230 | 15 | 0.99 | 5.5−5.6 | 4.2−4.3 |
| $0.063C_{AOM}POM_{CL}$ | 4.4 | 0.18 ± 0.004 | 0.68 ± 0.013 | 490 ± 27 | 15 | 1.00 | 5.4−5.5 | 4.4−4.5 |

[a] Note: ± corresponds to ± 1 standard deviation. Mass weighted $K_{fr}$ = sum (wt % * $K_{fr}$ for each fraction) = 1500 ± 130. wt %: weight fraction of subsample relative to composite; $f_{oc}$: organic carbon content; $N$: Freundlich exponent; $K_{fr}$: Freundlich constant; obs: number of observations for each isotherm; $K_{oc}$: organic carbon normalized sorption coefficient calculated at chemical equilibrium concentration ($C_e$) equal to 1 $\mu$g/L and 1 mg/L; 95% CI: 95% confidence interval.

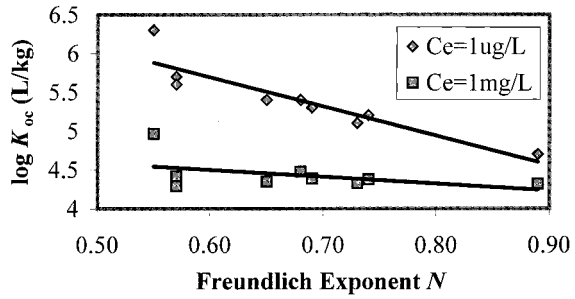


**FIGURE 3. Logarithm of organic content normalized distribution coefficient (log $K_{oc}$) versus Freundlich exponent ($N$) at chemical equilibrium concentrations ($C_e$) equal to 1 $\mu$g/L and 1 mg/L.**

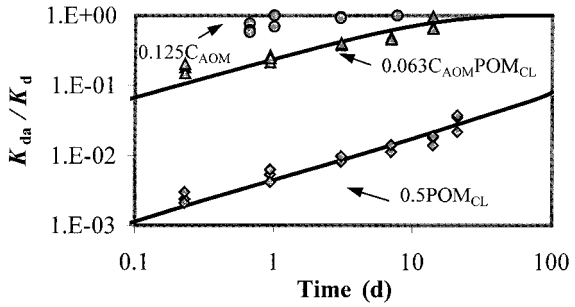


**FIGURE 4. The apparent sorption coefficient normalized by the equilibrium sorption coefficient ($K_{da}/K_d$) versus time (d) for three of the subsamples as well as the numerical model results for two of the subsamples. $K_d$ is the value extrapolated from the Freundlich equation based on the expected aqueous equilibrium concentration (given experimental parameters). The intraparticle model does not apply for sample ($0.125C_{AOM}$) because the process is not intraparticle diffusion and internal pore sorption but partitioning into the organic coatings on the exterior of the grains. Sample code: $XA_AB_B$ where X: size fraction; $A_A$: most dominant organic matter characteristic; $B_B$: second dominant organic matter characteristic; C: coating; AOM: amorphous organic matter; POM: particulate organic matter; CL: coal.**

based on the grain radii as described by Ball and Roberts (*20*). The diffusion rate constants represent transport both within the organic matter particles and the intraparticle pore space. For this reason grain radius might not always best describe the representative diffusion length.

The kinetic behavior of the two extreme but more homogeneous subsamples and a third heterogeneous sample (mixture of the two extremes) is presented in Figure 4. The fastest sorption kinetics was found in the subsample with AOM coatings ($0.125C_{AOM}$). The intraparticle diffusion model is not applied for this sample because the process is not intraparticle diffusion but partitioning into the organic coatings on the exterior of the grains. Sorption to this kind of organic matter is fast, as noted by other authors (*20*). The subsample dominated by POM (i.e. coal) ($0.5POM_{CL}$) is the slowest sample to reach sorption equilibrium, and the intraparticle diffusion model fits the data well (Figure 4). The POM radius in this sample is equal to the grain radius. The organic matter of the third subsample ($0.063C_{AOM}POM_{CL}$) is a mixture of two organic matter types (AOM coatings and coal), and its kinetic behavior is between that expected for subsamples dominated by each individual component. The intraparticle diffusion model does not fit the data as well for this third sample, fitting later data better than the earlier data. The earlier data fall above the model line suggesting the presence of a fast sorbing component in the sample (compare mean weighted squared error for this sample when including the first observation (0.120) versus ignoring this first data (0.027); Table 4).

Figure 5 presents various attempts to use the intraparticle diffusion model to fit the data for a mixed component subsample ($0.063C_{AOM}POM_{CL}$). Two different models were studied: (a) a one-component model (solid line in Figure 5), which assumes that the sample is homogeneous and all the components behave similarly, and (b) a two-component composite model (dashed line in Figure 5) which is actually a composite (superposition) of two individual components (I) a fast component (dotted line in Figure 5) and (II) a slow component (dashed−dotted line in Figure 5) portion. The relative weight percent of the fast and slow components was adjusted until the two-component model best agreed with the experimental data. When the fast and slow components were incorporated into the model, the two-component model line agreed with the data better than the one-component line. The two-component model fits the earlier data and at the same time captures the behavior of the slow component better than the one-component model. Figure 5 also presents the kinetic behavior for both the fast and the slow component, corroborating the previously mentioned hypothesis that the fast component affects the earlier time data—reaches equilibrium within 1 day—while the slow component dominates the later data. We thus recommend the use of the intraparticle diffusion model as a one-component model for homogeneous samples, while the use of a multicomponent model is required for heterogeneous samples {as suggested by Kleineidam et al. (*35*)}. Identifying the presence of organic coatings in the sample suggests the use of the two-component model.

The data in Table 4 also demonstrate the impact of having POM on sorption kinetics (see small apparent diffusion coefficient ($D_a$) values in Table 4). However, physical properties such as radius and intraparticle porosity are also important in interpreting the results. It is important to compare samples within the same grain size in order to draw conclusions on the effect of the organic matter type on

**TABLE 4. Kinetic Sorption Properties Based on Numerical Modeling[a]**

| sample code | *F* | *a* (cm) | $D_a/a^2$ (1/s) | $D_a$ (cm²/s) | T 75% (d) | error |
|---|---|---|---|---|---|---|
| CRA comp (actual sample) | 0.56 | 0.0077 | 7.7 E-08 | 4.6 E-12 | 12 | 0.046 |
| CRA comp (pulverized) | 0.27 | 0.0027 | 4.0 E-07 | 2.9 E-12 | 2 | 0.0023 |
| $0.5M_{AOM}POM_{PH}$ | 0.79 | 0.0180 | 1.4 E-09 | 4.5 E-13 | 490 | 0.079 |
| $0.5POM_{CL}$ | 0.98 | 0.0180 | 1.1 E-10 | 3.6 E-14 | 5700 | 0.040 |
| $0.25POM_{PH}M_{POM}$ | 0.80 | 0.0089 | 1.1 E-08 | 8.7 E-13 | 70 | 0.035 |
| $0.25M_{POM}$ | 0.55 | 0.0089 | 8.7 E-08 | 6.9 E-12 | 12 | 0.190 |
| $0.125C_{AOM}POM_{PH}$ | 0.73 | 0.0044 | 7.6 E-08 | 1.5 E-12 | 12 | 0.040 |
| $0.125C_{AOM}$ | 0.53 | 0.0044 | N/A | N/A | <1 | N/A |
| $0.063POM_{CH}C_{AOM}$ | 0.78 | 0.0027 | 3.7 E-08 | 2.8 E-13 | 20 | 0.042 |
| $0.063C_{AOM}POM_{CL}$ | 0.79 | 0.0027 | 7.2 E-08 | 5.4 E-13 | 12 | 0.120 (0.027)[b] |

[a] *F*: fractional uptake at equilibrium (chemical mass on solid per total chemical mass); *a*: grain radius used in the numerical model and is not the effective radius in all cases; $D_a/a^2$: apparent diffusion rate; $D_a$: apparent diffusion coefficient (based on the radius of the grain size fraction, in some samples the effective diffusion radius maybe different, data are only presented for comparison purposes); T 75%: time to reach 75% equilibrium; error: mean weighted squared error (*22*). [b] For sample ($0.063C_{AOM}POM_{CL}$) error in parentheses is the error calculated for the one-component model when the first observation is ignored. N/A: not analyzed intraparticle diffusion does not apply due to the partition nature of sorption in organic coatings.

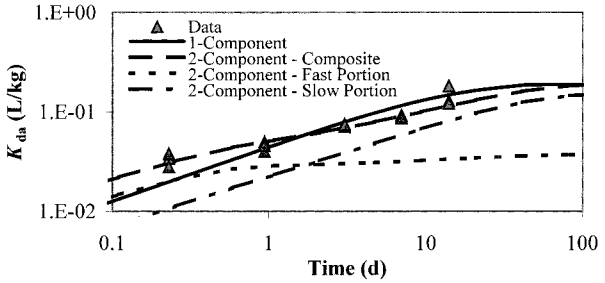


**FIGURE 5. Intraparticle diffusion model lines for one of the subsamples. Apparent sorption distribution coefficient ($K_{da}$) (L/kg) versus time (d). Two different models were studied: (a) a one-component model (solid line), which assumes that the sample is homogeneous and all the components behave similarly, and (b) a two-component composite model (dashed line) which is actually a composite (superimpose) of two individual components (I) a fast component (dotted line) and (II) a slow component (dashed−dotted line) portion.**

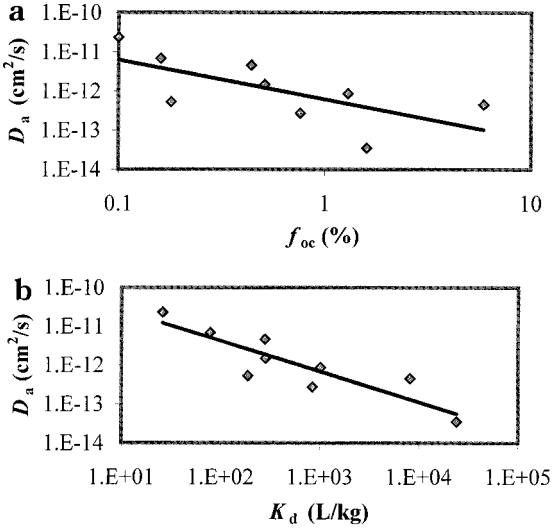


**FIGURE 6. Apparent diffusion coefficient ($D_a$) (cm²/s) versus (a) soil organic content $f_{oc}$ (%) and (b) sorption distribution coefficient $K_d$ (L/kg).**

sorption kinetics. For samples with phytoclast (e.g. $0.5M_{AOM}$-$POM_{PH}$, $0.25POM_{PH}M_{POM}$), the diffusion radius could be smaller than the actual radius since the phytoclast particles usually have cylindrical shape. The $D_a$ value calculated with the smaller radius could also be smaller than the actual one. For samples with POM in matrices (e.g. $0.25M_{POM}$), $D_a$ could be lower since the effective radius for POM is different from the grain size used. When comparing the three samples with AOM coatings and POM (i.e. $0.25POM_{PH}M_{POM}$, $0.063POM_{CH}C_{AOM}$, and $0.063C_{AOM}POM_{CL}$) the sample with the phytoclast is faster than the other two (see $D_a$ values in Table 4).

Figure 6a demonstrates that $D_a$ values decreased with increasing $f_{oc}$ in this research. However the data are highly scattered around the line that describes this inverse trend. The data scattering is decreased when $D_a$ is plotted against $K_d$ in Figure 6b. The data presented in Figure 6a,b illustrate that with increasing sorption more time is required to reach equilibrium (i.e. sorption reduces the effective diffusion rates and thus increases the time necessary to reach equilibrium). In this case, $f_{oc}$ alone is not enough to explain how sorption affects the effective diffusion coefficient; the $K_d$ value is more representative of the sorption behavior since more than one mechanism is affecting sorption in the subsamples. $D_a$ values are not true for all samples since the grain radius used in the numerical model is different for some samples than the effective radius. However, $D_a/a^2$ also follows the same trend, supporting the conclusion of diffusion-limited sorption.

Table 5 presents a qualitative comparison of the sorption characteristics for each organic matter group evaluated in the CRA. While we divide the samples into two main groups, (a) coaly POM and (b) young soil organic matter, some subsamples possess a mixture of these two groups. Coaly POM presents more nonlinear isotherms, higher $K_{oc}$ values, slower kinetics (Tables 3 and 4), and the sorption mechanism is site limited−site limited adsorption and/or pore filling, as

**TABLE 5. Qualitative Comparison of Organic Matter Sorption Characteristics**

| organic matter groups | petrography | isotherm | $K_{oc}$ | mechanism | kinetics |
|---|---|---|---|---|---|
| coaly particulate organic matter | particulate organic matter isolated and in clay matrices (coal, charcoal) | more nonlinear | high | adsorption (site limited) | slower |
| young soil organic matter | particulate organic matter (phytoclast), amorphous organic matter in clay matrices, and amorphous organic matter coatings | less nonlinear | low | partitioning | faster |
| mixture of two groups | mixed | nonlinear | intermediate | mixed | intermediate |

discussed in Chiou and Kile (*11*) and Xia and Ball (*12*). Young soil organic matter results in more linear sorption isotherms (or more linear than the coaly organic matter), lower $K_{oc}$ values that are close to $K_{ow}$-based estimates (4.4 for phenanthrene), faster sorption kinetics (Tables 3 and 4), and a partitioning sorption mechanism (*1, 12*). The mixture of these two groups tends to have the characteristics of the coaly POM. Even if the fraction percentage of the coaly POM is low, its impact on sorption behavior can be significant at low chemical concentrations (this study; *18*).

In summary, our observations demonstrate that even a fairly simple river alluvium sample can contain heterogeneous organic matter and that this heterogeneous organic matter can significantly impact sorption equilibrium and kinetics. In addition, we have shown that petrographic characteristics of the heterogeneous organic matter can help explain the variations in sorption properties. For example, the presence of coaly particles in a sample increases its sorption capacity, results in nonlinear sorption isotherms, and increases the equilibration time. Even small fractions of coaly materials can dominate the sorption capacity. Conversely, organic matter coatings have lower sorption capacities and equilibrate rapidly, requiring the addition of a fast sorption term in an intraparticle diffusion model. Recognizing the presence and importance of organic matter heterogeneities will facilitate interpretation of sorption data and could lead to prediction of sorption behavior for samples with heterogeneous organic matter.

## Acknowledgments

This study was partially funded by the U.S. National Science Foundation through the EPSCoR program. The authors would like to thank Renate Riehle for TOC measurements and Hermann Rügner for BET measurements, both from the Universität Tübingen. This research was conducted at the Universität Tübingen while D. A. Sabatini was on sabbatical there as a Senior Fulbright Scholar and while the first author, his Ph.D. student from the University of Oklahoma, was conducting research with him at the Universität Tübingen. Samples studied in this research were taken from the Norman Landfill Research Site, which is a U.S.G.S. Toxic Substances Research Site (http://wwwok.cr.usgs.gov/norlan/site.html). We acknowledge the assistance of Mr. Scott Christenson in obtaining samples from the site.

## Nomenclature

| | |
|---|---|
| $a$ | grain radius (cm) |
| AOM | amorphous organic matter |
| C | coatings |
| $C$ | chemical aqueous concentration |
| $C_e$ | equilibrium aqueous concentration of chemical ($\mu$g/L) |
| CH | charcoal |
| CL | coal |
| $D_a$ | apparent diffusion coefficient (cm$^2$/s) |
| $D_{aq}$ | aqueous diffusion coefficient (cm$^2$/s) |
| $D_a/a^2$ | diffusion rate constant (1/s) |
| $\epsilon$ | intraparticle porosity |
| F | fractional uptake at equilibrium (chemical mass on solid per total chemical mass) |
| $f_{oc}$ | fraction organic carbon content (%) |
| $K_d$ | sorption distribution coefficient (L/kg) |
| $K_{da}$ | apparent sorption distribution coefficient (L/kg) |
| $K_{fr}$ | Freundlich sorption constant [($\mu$g/kg)(L/$\mu$g)$^N$] |
| $K_{oc}$ | organic content normalized distribution coefficient (L/kg) |
| $K_{ow}$ | octanol−water partition coefficient |
| $N$ | Freundlich exponent |
| PH | phytoclast |
| POM | particulate organic matter |
| PV | pore volume for pore diameter <66.6 nm (cm$^3$/g) |
| $q_e$ | mass of chemical sorbed per mass of soil ($\mu$g/kg) |
| $\rho$ | bulk density |
| $r$ | radial distance from the center of the grain |
| SA | surface area (m$^2$/g) |
| $\tau_f$ | tortuosity factor |
| $t$ | time (d) |
| T 75% | time to reach 75% equilibrium (d) |
| wt % | weight fraction of composite (%) |

## Literature Cited

(1) Karickhoff, S. W.; Brown, D. S.; Scott, T. A. *Water Res.* **1979**, *13*, 241−248.
(2) Estrella, M. R.; Brusseau, M. L.; Maier, R. S.; Pepper, I. L.; Wierenga, P. J.; Miller, R. M. *Appl. Environ. Microbiol.* **1993**, *59*, 4266−4273.
(3) Chiou, C. T.; McGroddy, S. E.; Kile, D. E. *Environ. Sci. Technol.* **1998**, *32*, 264−269.
(4) Luthy, R. G.; Aiken, G. R.; Brusseau, M. L.; Cunningham, S. D.; Gschwend, P. M.; Pignatello, J. J.; Reinhard, M.; Traina, S. J.; Weber, W. J., Jr.; Westall, J. C. *Environ. Sci. Technol.* **1997**, *31*, 3341−3347.
(5) Barber, L. B.; Thurman, M. E.; Runnells, D. D. *J. Cont. Hydrol.* **1992**, *9*, 35−54.
(6) Weber, W. J., Jr.; McGinley, P. M.; Katz, L. E. *Environ. Sci. Technol.* **1992**, *26*, 1955−1962.
(7) Garbarini, D. R.; Lion, L. W. *Environ. Sci. Technol.* **1986**, *20*, 1263−1269.
(8) Grathwohl, P. *Environ. Sci. Technol.* **1990**, *24*, 1687−1693.
(9) Weber, W. J., Jr.; Huang, W. *Environ. Sci. Technol.* **1996**, *30*, 881−888.
(10) Xing, B.; Pignatello, J. J. *Environ. Sci. Technol.* **1997**, *31*, 792−799.
(11) Chiou, C. T.; Kile, D. E. *Environ. Sci. Technol.* **1998**, *32*, 338−343.
(12) Xia, G.; Ball W. P. *Environ. Sci. Technol.* **1999**, *33*, 262−269.
(13) Huang, W.; Weber, W. J., Jr. *Environ. Sci. Technol.* **1997**, *31*, 2562−2569.
(14) Young, T. M.; Weber, W. J., Jr. *Environ. Sci. Technol.* **1995**, *29*, 92−97.
(15) Leboeuf, E. J.; Weber, W. J., Jr. *Environ. Sci. Technol.* **1997**, *31*, 1697−1702.
(16) Graber, E. R.; Borisover, M. D. *Environ. Sci. Technol.* **1998**, *32*, 3286−3292.
(17) Chiou, C. T. *Environ. Sci. Technol.* **1995**, *29*, 1421−1422.
(18) Gustafsson, Ö.; Haghseta, F.; Chan, C.; MacFarlane, J.; Gschwend, P. M. *Environ. Sci. Technol.* **1997**, *31*, 203−209.
(19) Kleineidam, S.; Rügner, H.; Ligouis, B.; Grathwohl, P. *Environ. Sci. Technol.* **1999**, *33*, 1637−1644.
(20) Ball, W. P.; Roberts, P. V. *Environ. Sci. Technol.* **1991a**, *25*, 1237−1249.
(21) Grathwohl, P. *Diffusion in Natural Porous Media: Contaminant Transport, Sorption/Desorption and Dissolution Kinetics*; Kluwer Academic Publishers: Boston, MA, 1998.
(22) Rügner, H.; Kleineidam, S.; Grathwohl, P. *Environ. Sci. Technol.* **1999**, *33*, 1645−1651.
(23) Pignatello, J. J.; Xing, B. *Environ. Sci. Technol.* **1996**, *30*, 1−11.

(24) Grathwohl, P.; Reinhard, M. *Environ. Sci. Technol.* **1993**, *27*, 2360−2366.

(25) Harmon, T. C.; Roberts, P. V. *Environ. Sci. Technol.* **1994**, *28*, 1650−1660.

(26) Van Krevelen, D. W. *Coal Typology, Physics, Chemistry, and Constitution*, 3rd ed.; Elsevier: 1993.

(27) Tyson, R. V. *Sedimentary Organic Matter: Organic Facies and Palynofacies*; Chapman & Hall: London, 1995.

(28) Montgomery, J. H.; Welkom, L. M. *Ground Water Chemicals Desk Reference*; Lewis Publishers: Chelsea, MI, 1990.

(29) Ball, W. P.; Xia, G.; Durfee, D. P.; Wilson, R. D.; Brown, M..J.; Mackay, D. M. *GWMR* **1997**, *17*, 104−121.

(30) Karapanagioti, H. K.; Sabatini, D. A.; Kleineidam, S.; Grathwohl, P.; Ligouis, B. *Physics and Chemistry of the Earth* **1999**, *24*, 535−541.

(31) Jäger, R. *Modellierung Nichtlinear Intrapartikel-Diffusion in Heterogenem Aquifermaterial*; Diploma Thesis, University of Tübingen, FRG, 1997.

(32) Ball, W. P.; Roberts, P. V. *Environ. Sci. Technol.* **1991b**, *25*, 1223−1237.

(33) Barber, L. B. *Environ. Sci. Technol.* **1994**, *28*, 890−897.

(34) Schüth, C. Dissertation, University of Tübingen, FRG, 1994.

(35) Kleineidam, S.; Rügner, H.; Grathwohl, P. *Environ. Toxicol. Chem.* **1999**, accepted.

*Received for review February 24, 1999. Revised manuscript received November 1, 1999. Accepted November 8, 1999.*

ES9902219